The inhibitory mechanism of a small protein reveals its role in antimicrobial peptide sensing

Shan Jiang[1], Lydia C. Steup[1], Charlotte Kippnich[1], Symela Lazaridi[2,3], Gabriele Malengo[1], Thomas Lemmin[2] and Jing Yuan[1]*

Abstract

A large number of small membrane proteins have been discovered in bacteria, but their mechanism of action has remained mostly elusive. Here, we investigate the mechanism of a physiologically important small protein, MgrB, which represses the activity of the sensor kinase PhoQ and is widely distributed among enterobacteria. The PhoQ/PhoP two-component system is a master regulator of the bacterial virulence program and interacts with MgrB to modulate bacterial virulence, fitness, and drug resistance. A combination of crosslinking approaches with functional assays and protein dynamic simulations revealed structural rearrangements due to interactions between MgrB and PhoQ near the membrane/periplasm interface and along the transmembrane helices. These interactions induce the movement of the PhoQ catalytic domain and the repression of its activity. In the absence of MgrB, PhoQ appears to be insensitive to antimicrobial peptides, including the commonly used C18G. MgrB mediates the sensing of C18G by dissociating from and thus derepressing PhoQ. Our findings reveal the inhibitory mechanism of the small protein MgrB and uncover its importance in antimicrobial peptide sensing.

Significance Statement

Small proteins have been shown to have high prevalence, vast diversity and predominant regulatory functions in biological processes across all domains of life. However, their mechanisms of action remain largely elusive. In this study, we investigate the mechanism of the small protein, MgrB. It interacts with PhoQ sensor kinase, rearranges its conformation, represses its kinase activity and regulates bacterial response to environmental changes. Particularly for antimicrobial peptides, MgrB is required for bacteria to have a selective response to this host-exclusive stimulus. Our findings underline the importance of a small protein in bacterial fitness and drug resistance, provide a molecular basis for engineering novel peptide-based regulators, and present a framework for studying other small proteins.

Introduction

Small proteins are defined by their short sequence (usually < 50 aa) and their direct bio-generation via ribosomal translation. An increasing number of small proteins have been identified in individual species in all domains of life as well as in complex biological communities, suggesting a high prevalence and vast diversity in biological systems (reviewed in [1-4]). Many of these small proteins (~30%) are located in the cell membrane or have been predicted to be located there (e.g., [5, 6]). Although only a few detailed studies of small membrane proteins have been carried out, results show that small protein may target larger proteins and the lipid bilayer, regulating protein function, abundance, and changing membrane properties. This demonstrates thus their predominate role as regulators in the lipid bilayer (reviewed in [7]).

The membrane located PhoQ sensor kinase, a master regulator of bacterial virulence program, detects host-associated stimuli (review in [8]), such as cationic antimicrobial peptides (CAMPs) [9], mild acidic pH [10, 11], increased osmolarity [12], biliary unsaturated long-chain fatty acids [13], and magnesium limitation [14]. Three small membrane proteins have been identified to control PhoQ activity via direct protein-protein interactions. In *E. coli,* MgrB (47aa) and SafA (65aa) modulate PhoQ activity in the opposite direction, with MgrB acting as an inhibitor and SafA as an activator [15, 16]. Deletion of *mgrB* or *safA* resulted in *E. coli* cell division block under magnesium starvation or lowered acid resistance, respectively [17, 18]. In *Salmonella enterica* serovar Typhimurium, a species-specific small protein, UgtS (34aa), was discovered recently and shown to control the timing

of virulence gene expression by preventing premature PhoQ activation when inside macrophages [19].

PhoQ sensor kinase is found as a dimer on the bacterial inner membrane and consists of a periplasmic, a transmembrane (TM), a HAMP, a DHp and a catalytic domain. In the periplasmic domain, several molecular interactions are essential for the functional state of the PhoQ molecule. These include the central hydrogen bonding network (T48 D179 K186) in the PAS-fold [20-23], the inter-monomeric salt bridge (D179-R50')[24], the membrane-facing acidic patch and the juxta-membrane region at the periplasm/inner-membrane interface [9, 23, 25]. Mutations altering these molecular interactions change the conformation of the periplasmic domain and the sensitivity of PhoQ to magnesium, low pH, and CAMPs. Furthermore, distinct active states of the periplasmic domain were detected with different stimuli. For example, a PhoQ mutant that lost its sensitivity to low magnesium and low pH could still maintain its response to CAMPs [26]. In addition to the periplasmic domain, PhoQ transmembrane domain was shown to detect environmental osmotic upshifts, where the transmembrane four-helix bundle becomes more compact due to the increased membrane thickness and the lateral pressure in high osmolarity and adopts a kinase active conformation [12].

Among the known PhoQ-regulating small proteins, MgrB is the most widely distributed PhoQ repressor in enterobacteria. In *Salmonella*, the deletion of *mgrB* was shown to affect its infection of macrophages and epithelial cells [27]. In *Klebsiella pneumonia*, the disruption of the *mgrB* gene is the most prevalent among other chromosomal mutations in colistin-resistant strains [28]. Since the expression of *mgrB* is PhoPQ dependent, the inhibitory function of MgrB provides negative feedback to the two-component system [15, 29]. MgrB is a bitopic inner membrane protein with a short cytosolic N-terminus and a periplasmic C-terminal region (Fig. 1A). Two conserved cysteines (C28 and C39) in the periplasmic region have been shown to be important for MgrB function and have been hypothesized to form a disulfide bond [15]. This disulfide bond would also act as a sensor for the redox state of the bacterial periplasm creating an entry point for redox sensing by the PhoQ/PhoP system [30]. In addition to the two cysteines, eight functionally essential residues have been identified, spreading across the entire molecule [31]. However, the mechanism of MgrB inhibiting PhoQ remained largely unclear.

In this study, we used complementary approaches to identify PhoQ MgrB interactions, probe PhoQ conformational changes, and examine the impact of MgrB on PhoQ sensing environmental stimuli. We propose that the binding of MgrB (i) changes the conformation of the linker region between PhoQ periplasmic and transmembrane domains, (ii) changes the transmembrane four-helix bundle, and (iii) initiates the translocation of the catalytic domain. MgrB interferes with PhoQ signaling resulting in an overall lowered activity but still allows PhoQ activation under low pH, osmotic upshift, and magnesium limitation. We further reveal that MgrB mediates PhoQ sensing antimicrobial peptides, enabling bacteria to have a selective response to this exclusively host-associated stimulus.

Results

Disulfide crosslinking between MgrB and PhoQ TM helices

To identify interacting residues in PhoQ and MgrB, we started with the W20 in the transmembrane (TM) helix of MgrB, which was suggested to have direct contact with PhoQ [31]. Functional analysis of MgrB W20 variants (Fig. S1A) showed the wild-type-like activity of the MgrB W20Y variant, consistent with the predominant sequence conservation of W and Y at this position (Fig. S1B). The results implied that the nature of the interaction between MgrB and PhoQ at position 20 likely includes hydrophobic interactions via the aromatic ring structures and hydrogen bonding through

the hydroxyl group in tyrosine or the pyrrole moiety in tryptophan. Scanning through the sequence of the two PhoQ transmembrane helices, Y32 in TM1 appeared to be the optimal candidate to fulfill both types of interaction with MgrB W20.

To test this prediction with disulfide crosslinking, we generated the MgrB C16A W20C variant, which has only one cysteine residue in the transmembrane helix and constructed a PhoQ-TM_Cys library. A FLAG tag was fused to the N-terminus of MgrB to facilitate the detection of the PhoQ/MgrB complex with Western blot. Increased induction of MgrB C16A W20C was used (pTrc promoter with 10 µM IPTG) to ensure significant repression of PhoQ by the MgrB variant during crosslinking (Fig. S1C). When MgrB C16A W20C was co-expressed with PhoQ Y32C, we observed a higher molecular weight band at around 55 kDa on the Western blot corresponding to the PhoQ/MgrB complex (Fig. 1C), indicating the close proximity of MgrB W20 with the PhoQ TM1 residue Y32 in the complex. This band could be reduced by the addition of DTT and was absent when the cysteine residue was at position 16 (WT) or no cysteine was in the MgrB transmembrane helix (C16A). Additionally, we found that PhoQ L204C crosslinked with MgrB W20C, indicating MgrB position 20 near L204 in PhoQ TM2 as well (Fig. 1C).

Using MgrB residue 20 as a reference point, we next identified interacting amino acids of two more functionally important residues (Q22 and F24) in the MgrB TM helix [31]. In both cases, we observed stronger crosslinking bands and more than one crosslinked position in both transmembrane helices of PhoQ (Fig. 1D). For MgrB Q22C, stronger crosslinks were observed to residues in the PhoQ TM2 helix (colored blue). The strongest crosslinking band was shown when PhoQ Y197C was co-expressed. The crosslinking efficiency decreased when the cysteine residue moved to the neighboring positions and further away (196C, 195C, and 198C). It then got slightly stronger when the cysteine (194C) was roughly one helical turn away from Y197 (Fig. 1D left). Functionally, PhoQ Y197C complemented MgrB Q22C the most when compared to other PhoQ TM_Cys mutants, supporting the notion that MgrB Q22 primarily interacts with PhoQ Y197.

For MgrB F24C (Fig. 1D right), the highest crosslinking efficiency was found with a PhoQ TM1 mutant, I38C, which also functionally complemented MgrB F24C the most among the tested PhoQ/MgrB pairs. The minor crosslinking events observed could be due to the farther distance between the cysteine residues or an indication of intermediate binding states of MgrB. Collectively, we identified four-pair residues of MgrB and PhoQ, which are located in close proximity at the protein interface of the complex: W20-Y32, W20-L204, Q22-Y197, and F24-I38.

Crosslinking at the periplasmic domains of PhoQ and MgrB

To gain insights into PhoQ/MgrB interactions at the periplasmic domains, we attempted to identify interacting residue pairs using site-specific photo-crosslinking [32]. We introduced an amber stop codon at each residue in the MgrB periplasmic region (residues 25 to 47). The photo-crosslinking amino acid, *p*-benzoyl-l-phenylalanine (*p*Bpa), was then incorporated into the flag-tagged MgrB at the amber stop codon via the orthogonal $tRNA^{Amber}$ and the aminoacyl-tRNA synthetase during MgrB expression in *E. coli*. After UV irradiation, we detected bands with molecular weight ~55 kDa by anti-FLAG antibody when *p*Bpa was incorporated at positions 26, 30, 32, and 38, indicating the formation of the UV-dependent crosslinked PhoQ/MgrB complex (Fig. 2A and Fig. S2A). Among them, the crosslinked products from positions 30, 32 and 38 could be purified and subjected to mass spectrometry analysis (Fig. S2B and File S1). PhoQ was detected in all samples as the most prominent protein. Only a small number of other proteins were identified, indicating the protein purification steps were highly effective. MgrB was challenging to detect due to its small size, high hydrophobicity, and low number of potential MS-detectable peptides. However, increased sample injection amount allowed for the successful identification of MgrB in crosslinked complex samples, except when *p*Bpa was incorporated at position 38. This was most likely due to the incorporation of

*p*Bpa into the region of the small protein that resulted in the generation of detectable peptides in the other MgrB *p*Bpa variants. Despite the successful identification of both PhoQ and MgrB in the crosslinked bands, confident MS identification of MgrB-PhoQ crosslinked peptides providing clear evidence towards the positioning of the two proteins in the complex was not possible. The lack of crosslinked products with other *mgrB_amber* constructs could be due to the low efficiency of *p*Bpa incorporation (i.e., position 29) and the obstruction of the bulky unnatural amino acid on the binding of MgrB to PhoQ. Most of the residues showed crosslinked products are within the region flanked by the two highly conserved periplasmic cysteines (C28 and C39), suggesting the proximity and possibly direct interactions of MgrB C28-C39 region to PhoQ.

When placing the TM helices of PhoQ and MgrB in a membrane, the MgrB C28-C39 region would be spatially close to the PhoQ linker region connecting the periplasmic and the TM domains. This PhoQ linker region was previously shown to be functionally important. Mutation of residues in this region impaired the PhoQ response to magnesium and antimicrobial peptides [9, 23]. To test whether the MgrB C28-C39 region interacts directly with the linker region, we performed disulfide crosslinking with MgrB D31C and PhoQ_linker_Cys variants. As there are two essential cysteines in the MgrB periplasmic region, we first tested if introducing a third cysteine would affect MgrB function. We observed that the introduction of a third cysteine at position 31 did not reduce MgrB inhibition by MgrB as much as the C39A variant (Fig. S3), suggesting that the cysteine at position 31 does not severely interfere with the correct intra-MgrB disulfide bond formation and therefore suitable for the crosslinking experiments. The results showed that MgrB 31C formed disulfide linkages with cysteines in several different positions in the PhoQ linker region (184-188) with similar crosslinking efficiency (Fig. 2B). In the control experiment, where the wild-type MgrB was co-expressed with PhoQ_Cys mutants, no crosslinked products were observed. The data indicates that MgrB C28 and C39 were not involved in crosslinking with PhoQ and D31 is close to the PhoQ linker region. The comparable crosslinking efficiency at multiple positions is probably due to the flexible nature of PhoQ linker region and MgrB C28-C39.

The Alphafold models of the PhoQ/MgrB complex

To gain more detailed structural insights, we used Alphafold2 multimer [33-35] to predict the structures of the PhoQ/MgrB complex as well as the individual component of the complex (Fig. 3). The overall prediction of structural element fitted the previous experimental evidence. For example, the two conserved periplasmic cysteine residues (C28 and C39) in the MgrB structural model were in close proximity, structurally supporting the presence of a disulfide bond. In PhoQ, the PAS fold in the periplasmic domain, the HAMP, the DHp and the cytosolic catalytic domain resembled the experimental results of these structural elements [24, 36]. Unlike the asymmetric crystal structure of the PhoQ sensor domain [24], the Alphafold2 predicted PhoQ dimer was symmetric, which might represent only one of many PhoQ conformations.

In all five predicted PhoQ/MgrB complex models, MgrB was placed in between the PhoQ protomers, with the transmembrane helix parallel to the PhoQ TM helices. The two periplasmic cysteines formed a disulfide bond in four out of five predicted models or were in close proximity (3 Å apart). The transmembrane residue pairs, where disulfide crosslinking was observed, were positioned relatively close to each other with a distance ranging from 8.30 Å to 16.4 Å (Table 1). Disulfide crosslinking efficiency depends on several parameters, including the distance and the orientation of the sulfhydryl moiety, the dynamics of the residues and the accessibility of the oxidizing reagent. Experimentally, disulfide crosslinking was detected when the distance of two cysteines was below 15.2 Å [37]. All models predicted that the crosslinking pairs were less than 14 Å apart, except in model 5, where MgrB was positioned the farthest away from PhoQ. Furthermore, Q22-Y197 and F24-I38 pairs had shorter distances than the W20-Y32 and W20-L204 pairs. This is consistent with

our experimental results, where the former two pairs showed higher crosslinking efficiency than the latter. Model 5, however, does not fit with our experimental data and is likely to be an incorrect prediction.

When comparing the structural prediction of MgrB with its prediction in the complex, we observe that the helicity and rigidness of the C28-C39 region are greatly reduced, showing a more extended flexible loop conformation (Fig. 3D). This is in line with our observation that the bulky photo-activatable crosslinker *p*Bpa was able to incorporate into multiple positions in this region, and crosslinked to PhoQ. Furthermore, the predicted high level of flexibility of this region in the complex model agreed with our experimental data that the 31C in MgrB crosslinked with multiple sites in PhoQ with comparable efficiencies (Fig. 2B).

The conformational change of PhoQ linker region upon MgrB binding

We observe a good structural alignment when superposing the periplasmic domain (residue 41-181) of the PhoQ dimer to that of the monomer structure (Fig. S4A). In contrast, the positions of the TM helices upstream and downstream of this region diverged due to the different conformation of the linker region connecting the periplasmic and the TM domains in the two models. This linker region also showed a comparatively lower predicted local distance difference test loss (pLDDT) score, indicating a possible higher intrinsic flexibility of these residues (colored in yellow to green in Fig. S4A) and a higher capability of adopting different conformations. In particular, residues 187 and 188 located directly upstream of the PhoQ TM2 helix were in different conformations (loop vs. helix) in different PhoQ models (Fig S4B), potentially indicating their capability of large movements.

To detect conformational changes in the PhoQ linker region, we chose to focus on residues 187 and 188, which are located near the same lateral position as TM1 residue 43 (Fig. S4B). We observed that in the absence of MgrB, 43C and 188C formed an intramolecular disulfide linkage, showing as a faster-migrating band below the PhoQ monomer band (Fig. 4A). DTT treatment of the same sample brought the band back to the exact location as the PhoQ monomer, excluding the likelihood of protein degradation. Additionally, no PhoQ dimer band was detected in this condition, suggesting that 188C was not close to 43C' or the orientation of the 188C side chain was more toward the TM1 helix of the same protomer. In the presence of MgrB, the crosslinking pattern changed. The intramolecular crosslinking band reduced, and the intensity of the PhoQ dimer band increased, indicating the change in orientation or the distance of PhoQ residue 188 to residue 43 (Fig. 4B). The same trend of change was also observed for the residue 43 and 187 pair, but with reduced intramolecular crosslinking efficiency (Fig. S4). Our data suggest that MgrB binding changes the conformation of the PhoQ linker region connecting the periplasmic and the TM domains.

MgrB repression of PhoQ is divergent from high magnesium repression

Besides the small protein MgrB, high magnesium also represses PhoQ kinase activity [14]. The structural change of PhoQ under magnesium repression was studied in detail by monitoring the arrangement of α helices along the PhoQ dimer interface via disulfide-scanning [38]. It was proposed that under high magnesium conditions, the N-terminal α helix across the TM and the periplasmic domains undergoes a scissoring-type of motion with the pivot point near the periplasm/membrane interface [38].

Using a similar approach, we investigated the PhoQ dimer arrangement in the presence or absence of MgrB. Our data showed that most TM1 residues had reduced crosslinking between PhoQ dimers upon MgrB binding (Fig. 4C blue residues, Fig. S5). This was more prominent for residues near the membrane/cytoplasm interface, suggesting that MgrB binding pushes TM1-TM1' apart from each other and a propagation of PhoQ conformational change from periplasm to cytoplasm. In contrast, the presence of MgrB did not show a similar crosslinking effect on residues along the periplasmic helical interface (Fig. 4C purple residues, Fig. S5). Majority of residues in this region had little change

in crosslinking pattern. Some showed a significantly decreased (i.e., residues 46 and 60) or a slightly increased dimer fraction (i.e., residues 62). The overall PhoQ dimer rearrangement upon MgrB binding differs from the scissoring motion proposed for high magnesium repression, indicating that MgrB and high magnesium act differently on PhoQ. We then did functional analyses of PhoQ under high magnesium, with MgrB, or with both repressive factors. We observed that PhoQ was further repressed significantly when both high magnesium and MgrB were present (Fig. 4D), again supporting the notion that magnesium and MgrB have different mechanisms of repression.

MD simulations of PhoQ/MgrB complex models

When comparing predicted PhoQ dimer with its complex with MgrB, there was only minor conformational change. This is in stark contrast to the experimental results. We thus hypothesized that the Alphafold2 prediction might have only captured a transient arrangement of the complex but not a final state. To investigate the effect of MgrB on the dynamics of PhoQ, we carried out a set of four molecular dynamic simulations to investigate the effect of MgrB on the dynamics of PhoQ. The initial atomic models were obtained using the best ranked model predicted by the multimeric version of Alphafold2. In total, we modelled four different complexes: PhoQ (i) alone, and interacting with (ii) the wild-type MgrB, (iii) MgrB W20Y, a functional variant and (iv) MgrB W20A, an inactive variant. Each complex was inserted into a bacterial mimetic membrane bilayer and simulations were carried out up to 1 µs under near physiological conditions. All protein complexes remained stable throughout the entire simulations, with minor fluctuation in secondary structure. A principal component analysis of the transmembrane domain clearly showed that the wild-type MgrB and W20Y variant induced a similar conformational change (Fig. 5A), corresponding to an increase in the distance between PhoQ TM1, coupled with a decrease in distance between TM2. This change is more evident in TM residues near the membrane/cytoplasm interface (Fig. 5B and S6). The MgrB W20A had only a marginal impact on the conformation of the transmembrane domain.

In all the simulations with MgrB variants, we also observed the translocation of one of the PhoQ catalytic domains (Fig. 5C). This is most prominent in the simulations with the wild-type MgrB, where one catalytic domain moved fully away from the helix harboring the phosphorylatable histidine and located close to the inner membrane. For PhoQ alone, we did not observe any significant movement of the catalytic domains throughout the entire simulation. The functionally impaired MgrB W20A also induced PhoQ catalytic domain movement, though with less extent when compared to the wild type (Fig. 5C). In this simulation, the catalytic domain remained close to its initial position, but rotated by about 90°. Our previous study showed that the W20A mutant had reduced affinity to PhoQ and a relatively low activity [31]. However, since the simulation was seeded with a complex where MgrB W20A was already interacting with PhoQ, likely representing the scenario where the overexpression of MgrB W20A compensates for its weak binding to PhoQ and partially recovers its inhibitory function.

In sum, the simulation results support our experimental observations, showing the PhoQ structural changes at the MgrB binding site. Furthermore, the data showed that MgrB binding induces movements of the distantly located catalytic domain, suggesting the interference of MgrB on the signal transduction from the periplasmic/TM to the catalytic domains of PhoQ.

MgrB mediates PhoQ sensing cationic antimicrobial peptides

To study the impact of MgrB on PhoQ sensing stimuli, we tested PhoQ activation by low pH, osmotic upshift, and cationic antimicrobial peptides with the GFP reporter assay. PhoQ was activated at pH 5.5 or with 300 mM NaCl but not with the antimicrobial peptide C18G in the presence of high magnesium (10 mM), consistent with previous reports [9, 10, 12]. The activation did not appear to change much when MgrB was absent, except that the overall PhoQ activity increased due to the lack of MgrB repression (Fig. 6A). We next followed PhoQ activity in the presence of antimicrobial

peptide LL37 and C18G under non-inhibitory magnesium conditions (1 mM). We observed up to a nearly 5-fold increase of PhoQ activity by antimicrobial peptides when the wild-type MgrB was present. However, in the absence of functional MgrB, almost no PhoQ activation was observed, indicating MgrB is required for PhoQ to sense antimicrobial peptides under low magnesium (Fig. 6B).

The lack of PhoQ activation without MgrB might also be due to the protective effect of the overall higher activity of the PhoQ/PhoP two-component system, which could increase the outer membrane modification and reduce the entry of antimicrobial peptides to the periplasm. To have more direct evidence, we monitored PhoQ and MgrB interactions *in vivo* using the acceptor photobleaching Förster resonance energy transfer (FRET) approach. PhoQ and MgrB fused with fluorescent proteins (PhoQ-mNeonGreen and mCherry-MgrB) were expressed in *E. coli*. Cells were collected in the mid-log phase, treated with C18G, and then used for FRET measurements (Fig. 6C). The control cells without C18G treatment, showed energy transfer from mNeonGreen to mCherry with about 10% efficiency, comparable to our previous report [12], indicating the formation of the PhoQ/MgrB complex *in vivo*. With the C18G treatment, the FRET efficiency reduced to about 2%, slightly higher than the negative controls, suggesting that antimicrobial peptides cause the dissociation of PhoQ from its small protein inhibitor MgrB. Cumulatively, our data strongly support that MgrB mediates the antimicrobial peptide sensing by PhoQ.

Discussions

The PhoQ/PhoP two-component system regulates the expression of a large set of genes and is essential for bacteria to respond to environmental stresses and their mammalian hosts. Constitutive PhoQ activity was shown to lead to the attenuation of Salmonella virulence [39]. In *E. coli*, increased PhoQ activity may result in fitness disadvantages due to the large size of the PhoP regulon or cause cell division block when PhoQ is strongly stimulated [17]. MgrB represses PhoQ, providing negative feedback and maintaining a proper activity level of the system. In this study, we report that MgrB directly interacts with the PhoQ TM and the sensor/TM linker region, interfering with the signaling of PhoQ. It reduces the overall activity of PhoQ yet still allows activation by low magnesium, low pH, increased osmolarity, and CAMPs. We further reveal that PhoQ activation by CAMPs is MgrB-dependent under physiologically relevant magnesium conditions (1 mM). MgrB derepresses PhoQ by dissociating from it in the presence of antimicrobial peptides. This allows a higher PhoQ activity, an increase in outer membrane modification, and thus an elevated resistance against CAMPs. Since the septum is the initial attacking site of CAMPs (i.e., LL37) on the membrane [40], the division block caused by strong PhoQ activation becomes the protection for counteracting the killing of host innate immunity.

In contrast to sensing extracellular low pH and magnesium limitation, the sensing of CAMPs by PhoQ was shown to be required for *Salmonella* infecting mammalian hosts [26]. CAMPs were suggested to bind to the acidic patch in the PhoQ periplasmic domain [9], which is relatively distant from the MgrB binding site and unlikely to compete with MgrB directly. It is more plausible that the binding of CAMPs causes PhoQ conformational change and leads to the dissociation of MgrB from PhoQ. We observed that a high level of magnesium (10 mM) repressed PhoQ activation by CAMPs in the presence or absence of MgrB in *E. coli*, consistent with the previous report in *Salmonella*, even though MgrB had not yet been discovered at that time [9]. The same report proposed that CAMPs activate PhoQ by replacing magnesium ions from the acidic patch in PhoQ, which is different from our MgrB-mediated CAMP sensing mechanism. Both hypotheses, however, are not in conflict with each other but rather describe two aspects of PhoQ sensing CAMPs under different magnesium conditions. Furthermore, a recent study revealed that antimicrobial peptides with ß-sheet structure or neutral charge could also activate PhoQ [54]. These newly found PhoQ activators do not possess

the properties to interact with the PhoQ acidic patch. Additionally, there are PhoQ homologs that do not have an acidic patch in their sequences. Our mechanism provides a suitable explanation for both cases, where antimicrobial peptide sensing cannot be explained by the other model.

By monitoring PhoQ conformational change and activities, we show that MgrB repression is divergent from high magnesium repression. We also observed that PhoQ could be further repressed when both high magnesium and MgrB are present. This is consistent with the different binding sites of magnesium and MgrB on PhoQ. Magnesium was suggested to bind to several locations, including the acidic patch near the inner membrane (148-152) and residues G93, W97, H120, and T156 [14, 23, 41]. Mutations of these residues were shown to abolish magnesium protection from iron-mediated cleavage [41]. The majority of these residues are located in the peripheral of the periplasmic domain, distinct from the MgrB binding site.

Our crosslinking results revealed extensive interactions between PhoQ and MgrB in the juxta-membrane region, implying that the linker region between the PhoQ sensor and TM domains is a hotspot for functional regulations. Highly conserved and functionally important residues are found in or near this region, such as K186, T48, R50, E184, and L185, whose mutations lead to alterations in PhoQ activity as well as signaling capability [20, 23, 24]. Curiously, the wild-type MgrB maintained its inhibition on PhoQ linker variants, suggesting the flexibility of the MgrB loop and the possible various interaction modes between the MgrB loop and the PhoQ linker regions. This is consistent with our observations that multiple residues in the PhoQ linker region crosslinked with one residue in the MgrB loop with comparable efficiency. Interestingly, the PhoQ activating protein, SafA, appears to act near this linker region in terms of the closely located putative SafA binding site and the inter-monomeric salt bridge (R50'-D179), which is required for SafA activation [42, 43]. Whether MgrB repression competes with SafA activation of PhoQ and how these regulations are coordinated, await further studies.

Sensor kinases in bacterial two-component systems are evolutionarily related and have structural resemblance. We found that the predicted structures of EnvZ, QseC, and CreC sensor kinases closely resemble the PhoQ structure. EnvZ was also shown to form a complex with MgrB experimentally [31]. Together with the mechanism of MgrB revealed here, it is foreseeable that novel small protein regulators can be designed for PhoQ, EnvZ, and possibly many other sensor kinases. This will contribute to the repertoire of new antimicrobial agents targeting sensor kinases that regulates bacterial virulence [45] and to the treatment of infections caused by drug-resistant pathogens.

Materials and methods

Bacterial strains, plasmids, and growth conditions

The complete lists of strains, plasmids, and primers used in this study are summarized in Table S1, S2, and S3, respectively. The *E. coli* MG1655 *ΔmgrB* and *ΔphoQΔmgrB* strains were from the previous study [31]. All strains were grown in the lysogeny broth (LB) medium at 37 ^{o}C with shaking unless otherwise indicated. Genes in pTrc99a vector were induced with isopropyl β-D-1-thiogalactopyranoside (IPTG) at a final concentration of 10 μM. Genes in pBAD vector were induced with 0.008% arabinose. Genes in pEVOL-pBpF vector were induced with 0.02% arabinose. Genes in pETduet-1 vector were induced with IPTG at a final concentration of 0.5 mM. When appropriate, the antibiotics ampicillin, kanamycin, and chloramphenicol were used at concentrations of 100 μg/mL, 50 μg/mL, and 34 μg/mL, respectively. A detailed description of cloning and plasmid construction can be found in the SI Materials and Methods.

Disulfide crosslinking *in vivo*

The *in vivo* disulfide-crosslinking experiments were performed as previously described with modifications [46]. Briefly, cells carrying pBAD33 *phoQ* variant and pTrc99A *mgrB* variant were grown at 37 °C in LB medium supplemented with 10 mM $MgSO_4$ overnight, then diluted 1:100 to fresh LB medium supplemented with 1 mM $MgSO_4$. The expression of plasmid-encoded proteins was induced with arabinose and IPTG. When the OD_{600} value reached 0.6, cells were harvested, washed, and resuspended in the crosslinking buffer (137 mM NaCl, 2.7 mM KCl, 10 mM Na_2HPO_4, 1.8 mM KH_2PO_4, 1mM $MgSO_4$, and 0.1 mM Cu-phenanthroline), followed by 10 minutes incubation at 25 °C. The reaction was stopped by pelleting the cells and then resuspending in the 1x stop-solution (8 mM sodium phosphate buffer, pH 7.8, 12.5 mM EDTA, and 12.5 mM N-ethylmaleimide) and incubation at 25 °C for 10 minutes. Cells were collected, resuspended in the lysis buffer (50 mM Tris-HCl, pH 8.0, 100 mM NaCl, and protease inhibitors), mixed with lysing matrix B beads (MP Biomedicals), and broken with a homogenizer following the manufacturer's instructions. The mixture was spun down at 2,300 x g for 10 minutes at 4 °C to pellet the beads and cell debris. The supernatant was centrifuged at 21,000 x g for one hour at 4 °C to pellet the membrane fraction, which was then dissolved in the SDS sample buffer at 4 °C overnight. The membrane proteins were separated on an SDS tris-tricine or tris-glycine polyacrylamide gel via electrophoresis and analyzed with Western blot.

Western blot analysis

Proteins were transferred from a polyacrylamide gel to a polyvinylidene fluoride membrane or nitrocellulose membrane. PhoQ-His and Flag-MgrB were detected with the anti-His and anti-Flag primary antibody (Sigma), respectively. The IRDye 800CW-conjugated secondary antibody (LI-COR) was used, and the protein bands were visualized with the Odyssey CLx imaging system (LI-COR) and quantified with ImageJ.

Functional assay with the *gfp* reporter gene

The GFP reporter assay was performed as described before [12]. Briefly, the reporter plasmid pUA66 *PmgtLA-gfp* was transformed to strains indicated. The resulting transformants were grown overnight at 37 °C in LB medium with 10 mM $MgSO_4$, then diluted 1:100 to fresh LB medium with magnesium and inducers as indicated. The cultures were grown at 37 °C with vigorous shaking till the early log phase (OD=0.4-0.5). The fluorescence of cells was monitored with a BD LSRFortessa SORP flow cytometer (BD Biosciences) equipped with a 100-mW 488-nm laser and a 510/20 bandpass filter. BD FACSDiva software version 8.0 (BD Biosciences) was used to analyze the acquired data.

Unnatural amino acid incorporation in MgrB and site-specific UV crosslinking *in vivo*

The site-specific photo-crosslinking experiments were performed as described before with modifications [32, 47]. *E. coli* BL21 DE3 cells carrying pETduet-1 *phoQ-his$_6$ flag-mgrB* and pEVOL-pBpF vectors were grown in LB medium at 37 °C overnight, then diluted 1:100 to fresh LB medium containing 0.5 mM p-benzoyl-l-phenylalanine (pBpA). When the OD_{600} value reached around 0.6, cells were induced with arabinose (0.02%) and IPTG (0.5 mM) for 4h at 30 °C, followed by harvesting, washing two times, and resuspension in 1 ml cold PBS buffer. The bacterial suspension was spread out onto a 35 mm round dish on ice and irradiated for 5 minutes with 365 nm UV light using an LED UV hand lamp (Honle UV technology). Cells were then harvested at 4 °C, and the formation of crosslinked PhoQ/MgrB complex was then detected by the separation of total protein with polyacrylamide gel electrophoresis and Western blot with anti-Flag antibody. The crosslinked complex was purified by affinity chromatography, separated in an SDS polyacrylamide gel, and verified by mass spectrometry (see SI Materials and Methods for details).

Molecular modeling and Molecular dynamics simulations

The PhoQ/MgrB complex was modeled using Alphafold2 multimer on Colab [PMID: 35637307]. We considered four difference complexes: i. PhoQ, ii. PhoQ / MgrB, iii. PhoQ / MgrB W20Y variant, and iv. PhoQ / MrgB W20A variant. Each complex was inserted into a bacterial membrane mimetic

composed of a mixture of phosphatidylethanolamine (POPE) and phosphatidylglycerol (POPG) with a 3:1 ratio. The systems were solvated with a 17 Å water padding and neutralized with NaCl at a concentration of 150 mM. Each system was assembled using the CHARMM-GUI webserver [48].

The simulation was performed with the CHARMM36m force field, including CMAP corrections for the protein [49]. The water molecules were described with the TIP3P water parameterization [50]. The simulations were carried out with OPENMM molecular engine [51] following the minimization and equilibration protocols provided by CHARMM-GUI. The cutoff for non-bonded interactions was set to 12 Å with a switching distance at 10 Å. The periodic electrostatic interactions were computed using particle-mesh Ewald (PME) summation with a grid spacing smaller than 1 Å. Constant temperature of 310 K was imposed by Langevin dynamics with a damping coefficient of 1.0 ps. Constant pressure of 1 atm was maintained with Monte Carlo barostat [52]. The hydrogen mass repartitioning scheme was used to achieve a 4 fs time-step [53]. The simulations were carried out up to 1 µs.

Acceptor photobleaching FRET analysis

FRET measurements were performed as described before [31]. The expression of PhoQ-mNeonGreen and mCherry-MgrB was induced in *E. coli* lptD4213 strain with 0.008% arabinose and 10 µM IPTG, respectively. The cultures were grown to the mid-log phase (OD=0.6) in LB media. Cells were harvested and washed twice with pre-chilled tethering buffer (20 mM potassium phosphate pH 7.0, 1 µM methionine, 10 mM lactic acid, and 10 mM magnesium sulfate). The surface of a glass-bottom 96-well plate (Greiner) was treated with 0.1% poly-L-lysine for 15 minutes at room temperature, followed by removing poly-L-Lysine and air-dry for 5 minutes. The wells were washed twice using a pre-chilled tethering buffer. Subsequently, cells were incubated in the wells at room temperature for 25 minutes to allow attachment. Unattached cells were removed by washing with tethering buffer twice, and attached cells were overlaid with tethering buffer with or without 10 µg/ml C18G and incubated at room temperature for one hour. Acceptor photobleaching FRET was performed using the same microscope settings previously [31]. The details of the data acquisition and analysis can be found in the SI Materials and Methods.

Acknowledgments

We thank L. Cassidy and A. Throley for performing mass spectrometry analyses; H. Koch for pEVOL-pBpF vector and the site-directed photo-crosslinking protocol; M. Stopp for the disulfide crosslinking protocol; S. G. Sierra for technical assistance; members of the Yuan and the Sourjik laboratories for helpful discussions.

This work is supported by the German Research Foundation (DFG) priority program 2002 YU 247/3-1 and the Max Planck Society (to J.Y.), the Swiss National Science Foundation (SNSF) award PCEFP3_194606 (to T.L. and S.L.).

J.Y. and T.L. designed the experiments; S.J., L.C.S., C.K., S.L., and J.Y. performed the experiments; S.J., G.M., L.C.S., C.K., S.L., T.L., V.S., and J.Y. analyzed data; J.Y., T.L., and S.J. wrote the manuscript.

References

1. Duval, M. and P. Cossart, *Small bacterial and phagic proteins: an updated view on a rapidly moving field.* Curr Opin Microbiol, 2017. **39**: p. 81-88.
2. Ramamurthi, K.S. and G. Storz, *The small protein floodgates are opening; now the functional analysis begins.* BMC Biol, 2014. **12**: p. 96.

3. Su, M., et al., *Small proteins: untapped area of potential biological importance.* Front Genet, 2013. **4**: p. 286.
4. Weidenbach, K., et al., *Small Proteins in Archaea, a Mainly Unexplored World.* J Bacteriol, 2022. **204**(1): p. e0031321.
5. Sberro, H., et al., *Large-Scale Analyses of Human Microbiomes Reveal Thousands of Small, Novel Genes.* Cell, 2019. **178**(5): p. 1245-1259 e14.
6. Hemm, M.R., J. Weaver, and G. Storz, *Escherichia coli Small Proteome.* EcoSal Plus, 2020. **9**(1).
7. Yadavalli, S.S. and J. Yuan, *Bacterial Small Membrane Proteins: the Swiss Army Knife of Regulators at the Lipid Bilayer.* J Bacteriol, 2022. **204**(1): p. e0034421.
8. Groisman, E.A., A. Duprey, and J. Choi, *How the PhoP/PhoQ System Controls Virulence and Mg(2+) Homeostasis: Lessons in Signal Transduction, Pathogenesis, Physiology, and Evolution.* Microbiol Mol Biol Rev, 2021. **85**(3): p. e0017620.
9. Bader, M.W., et al., *Recognition of antimicrobial peptides by a bacterial sensor kinase.* Cell, 2005. **122**(3): p. 461-72.
10. Prost, L.R., et al., *Activation of the bacterial sensor kinase PhoQ by acidic pH.* Mol Cell, 2007. **26**(2): p. 165-74.
11. Choi, J. and E.A. Groisman, *Acidic pH sensing in the bacterial cytoplasm is required for Salmonella virulence.* Mol Microbiol, 2016. **101**(6): p. 1024-38.
12. Yuan, J., et al., *Osmosensing by the bacterial PhoQ/PhoP two-component system.* Proc Natl Acad Sci U S A, 2017. **114**(50): p. E10792-E10798.
13. Carabajal, M.A., et al., *PhoQ is an unsaturated fatty acid receptor that fine-tunes Salmonella pathogenic traits.* Sci Signal, 2020. **13**(628).
14. Garcia Vescovi, E., F.C. Soncini, and E.A. Groisman, *Mg^{2+} as an extracellular signal: environmental regulation of Salmonella virulence.* Cell, 1996. **84**(1): p. 165-74.
15. Lippa, A.M. and M. Goulian, *Feedback inhibition in the PhoQ/PhoP signaling system by a membrane peptide.* PLoS Genet, 2009. **5**(12): p. e1000788.
16. Eguchi, Y., et al., *B1500, a small membrane protein, connects the two-component systems EvgS/EvgA and PhoQ/PhoP in Escherichia coli.* Proceedings of the National Academy of Sciences of the United States of America, 2007. **104**(47): p. 18712-18717.
17. Yadavalli, S.S., et al., *Antimicrobial peptides trigger a division block in Escherichia coli through stimulation of a signalling system.* Nat Commun, 2016. **7**: p. 12340.
18. Eguchi, Y., et al., *Regulation of acid resistance by connectors of two-component signal transduction systems in Escherichia coli.* J Bacteriol, 2011. **193**(5): p. 1222-8.
19. Salvail, H., J. Choi, and E.A. Groisman, *Differential synthesis of novel small protein times Salmonella virulence program.* PLoS Genet, 2022. **18**(3): p. e1010074.
20. Sanowar, S., A. Martel, and H.L. Moual, *Mutational analysis of the residue at position 48 in the Salmonella enterica Serovar Typhimurium PhoQ sensor kinase.* J Bacteriol, 2003. **185**(6): p. 1935-41.
21. Regelmann, A.G., et al., *Mutational analysis of the Escherichia coli PhoQ sensor kinase: differences with the Salmonella enterica serovar Typhimurium PhoQ protein and in the mechanism of Mg2+ and Ca2+ sensing.* J Bacteriol, 2002. **184**(19): p. 5468-78.
22. Minagawa, S., et al., *Isolation and molecular characterization of the locked-on mutant of Mg2+ sensor PhoQ in Escherichia coli.* Biosci Biotechnol Biochem, 2005. **69**(7): p. 1281-7.

23. Cho, U.S., et al., *Metal bridges between the PhoQ sensor domain and the membrane regulate transmembrane signaling.* J Mol Biol, 2006. **356**(5): p. 1193-206.
24. Cheung, J., et al., *Crystal structure of a functional dimer of the PhoQ sensor domain.* J Biol Chem, 2008. **283**(20): p. 13762-70.
25. Waldburger, C.D. and R.T. Sauer, *Signal detection by the PhoQ sensor-transmitter. Characterization of the sensor domain and a response-impaired mutant that identifies ligand-binding determinants.* J Biol Chem, 1996. **271**(43): p. 26630-6.
26. Hicks, K.G., et al., *Acidic pH and divalent cation sensing by PhoQ are dispensable for systemic salmonellae virulence.* Elife, 2015. **4**: p. e06792.
27. Venturini, E.S., S. L.; Maaß, S.; Gelhausen, R.; Eggenhofer, F.; Li, L.; Cain, A. K.; Parkhill, J.; Becher, D.; Backofen, R.; Barquist, L.; Sharma, C. M.; Westermann, A. J.; Vogel, J., *A global data-driven census of Salmonella small proteins and their potential functions in bacterial virulence.* microLife, 2020. **1**(1).
28. Shein, A.M.S., et al., *High prevalence of mgrB-mediated colistin resistance among carbapenem-resistant Klebsiella pneumoniae is associated with biofilm formation, and can be overcome by colistin-EDTA combination therapy.* Sci Rep, 2022. **12**(1): p. 12939.
29. Salazar, M.E., A.I. Podgornaia, and M.T. Laub, *The small membrane protein MgrB regulates PhoQ bifunctionality to control PhoP target gene expression dynamics.* Mol Microbiol, 2016. **102**(3): p. 430-445.
30. Lippa, A.M. and M. Goulian, *Perturbation of the oxidizing environment of the periplasm stimulates the PhoQ/PhoP system in Escherichia coli.* J Bacteriol, 2012. **194**(6): p. 1457-63.
31. Yadavalli, S.S., et al., *Functional determinants of a small protein controlling a broadly conserved bacterial sensor kinase.* J Bacteriol, 2020.
32. Ryu, Y. and P.G. Schultz, *Efficient incorporation of unnatural amino acids into proteins in Escherichia coli.* Nat Methods, 2006. **3**(4): p. 263-5.
33. Mirdita, M., et al., *ColabFold: making protein folding accessible to all.* Nat Methods, 2022. **19**(6): p. 679-682.
34. Evans, R., et al., *Protein complex prediction with AlphaFold-Multimer.* bioRxiv, 2022: p. 2021.10.04.463034.
35. Akdel, M., et al., *A structural biology community assessment of AlphaFold2 applications.* Nat Struct Mol Biol, 2022. **29**(11): p. 1056-1067.
36. Ferris, H.U., et al., *Mechanism of regulation of receptor histidine kinases.* Structure, 2012. **20**(1): p. 56-66.
37. Careaga, C.L. and J.J. Falke, *Thermal motions of surface alpha-helices in the D-galactose chemosensory receptor. Detection by disulfide trapping.* J Mol Biol, 1992. **226**(4): p. 1219-35.
38. Molnar, K.S., et al., *Cys-scanning disulfide crosslinking and bayesian modeling probe the transmembrane signaling mechanism of the histidine kinase, PhoQ.* Structure, 2014. **22**(9): p. 1239-1251.
39. Miller, S.I. and J.J. Mekalanos, *Constitutive expression of the phoP regulon attenuates Salmonella virulence and survival within macrophages.* J Bacteriol, 1990. **172**(5): p. 2485-90.
40. Sochacki, K.A., et al., *Real-time attack on single Escherichia coli cells by the human antimicrobial peptide LL-37.* Proc Natl Acad Sci U S A, 2011. **108**(16): p. E77-81.

41. Chamnongpol, S., M. Cromie, and E.A. Groisman, *Mg2+ sensing by the Mg2+ sensor PhoQ of Salmonella enterica.* J Mol Biol, 2003. **325**(4): p. 795-807.
42. Eguchi, Y., et al., *The connector SafA interacts with the multi-sensing domain of PhoQ in Escherichia coli.* Mol Microbiol, 2012. **85**(2): p. 299-313.
43. Yoshitani, K., et al., *Identification of an internal cavity in the PhoQ sensor domain for PhoQ activity and SafA-mediated control.* Biosci Biotechnol Biochem, 2019. **83**(4): p. 684-694.
44. Akdel, M., et al., *A structural biology community assessment of AlphaFold2 applications.* Nat Struct Mol Biol, 2022.
45. Cabezudo, I., et al., *Effect-Directed Synthesis of PhoP/PhoQ Inhibitors to Regulate Salmonella Virulence.* J Agric Food Chem, 2022. **70**(22): p. 6755-6763.
46. Stopp, M., et al., *Transmembrane signaling and cytoplasmic signal conversion by dimeric transmembrane helix 2 and a linker domain of the DcuS sensor kinase.* J Biol Chem, 2021. **296**: p. 100148.
47. Kuhn, P., et al., *Ribosome binding induces repositioning of the signal recognition particle receptor on the translocon.* J Cell Biol, 2015. **211**(1): p. 91-104.
48. Jo, S., et al., *CHARMM-GUI: a web-based graphical user interface for CHARMM.* J Comput Chem, 2008. **29**(11): p. 1859-65.
49. Best, R.B., et al., *Optimization of the additive CHARMM all-atom protein force field targeting improved sampling of the backbone phi, psi and side-chain chi(1) and chi(2) dihedral angles.* J Chem Theory Comput, 2012. **8**(9): p. 3257-3273.
50. Jorgensen, W.L., Chandrasekhar, J., and Madura, J. D., *Comparison of simple potential functions for simulating liquid water.* J Chem Phys, 1983. **79**(2).
51. Eastman, P., et al., *OpenMM 7: Rapid development of high performance algorithms for molecular dynamics.* PLoS Comput Biol, 2017. **13**(7): p. e1005659.
52. Chow, K.a.F., D. M. , *Isothermal-isobaric molecular dynamics simulations with Monte Carlo volume sampling.* Comp. Phys. Comm., 1995. **91**(1-3): p. 283-289.
53. Balusek, C., et al., *Accelerating Membrane Simulations with Hydrogen Mass Repartitioning.* J Chem Theory Comput, 2019. **15**(8): p. 4673-4686.
54. Brink, K.R., et al., *An E. coli display method for characterization of peptide-sensor kinase interactions.* Nat Chem Biol, 2022.

Figures and tables

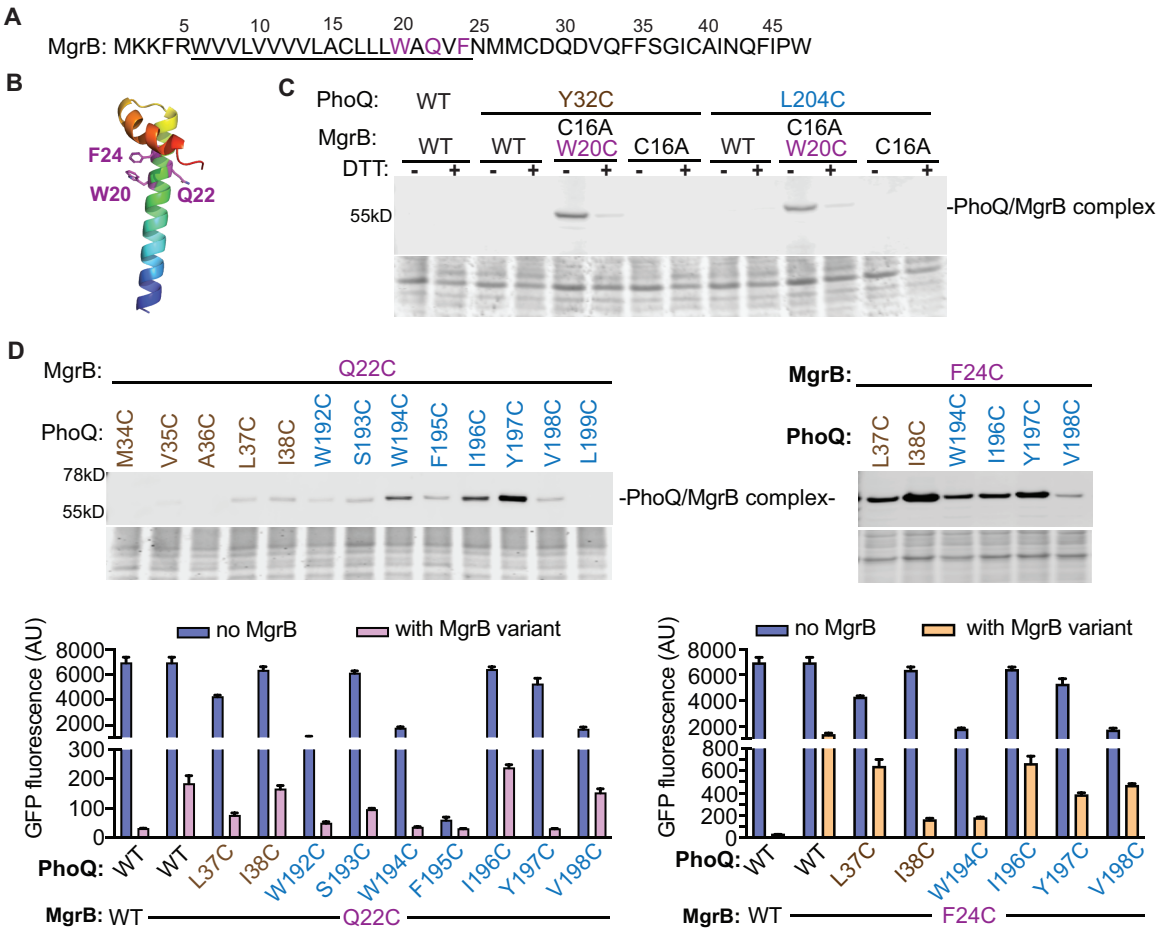

Fig. 1. Identification of the interacting residues between MgrB and PhoQ in the TM helices. (**A**) The sequence of MgrB from *E. coli*. Residues predicted to be in the transmembrane helix are underlined. (**B**) The tertiary structure of MgrB predicted by Alphafold2 is shown in ribbon with rainbow spectrum. The protein N-terminus is colored in blue and C-terminus in red. The positions involved in crosslinking (20, 22 and 24) are in purple and shown with sided chains in ball and stick. (**C, D top**) Western blot analysis of *E. coli* membrane extracts after disulfide crosslinking. The indicated PhoQ and FLAG-tagged MgrB variants were expressed in *E. coli*, followed by Cu-phenanthroline catalyzed the disulfide crosslinking (details in Materials and Methods). The total protein stain of the PVDF membranes serves as loading control. Residues from PhoQ TM1 and TM2 are colored in wheat and blue, respectively. Magenta indicates the residues in the MgrB TM helix. Data are representative of at least three independent experiments**. (D bottom**) The functional assay of PhoQ Cys-variants with or without MgrB. An GFP reporter plasmid carrying the *gfp* gene fused with a PhoP regulated promoter P_{mgtLA} was introduced to the *E. coli* strain. The expression of *phoQ* and *mgrB* variants was induced and cells were grown to the early log phase. Then the function of PhoQ variants was monitored by measuring the GFP reporter fluorescence of the cell culture. Each data point is shown with the calculated average and standard deviation from three independent biological replicates.

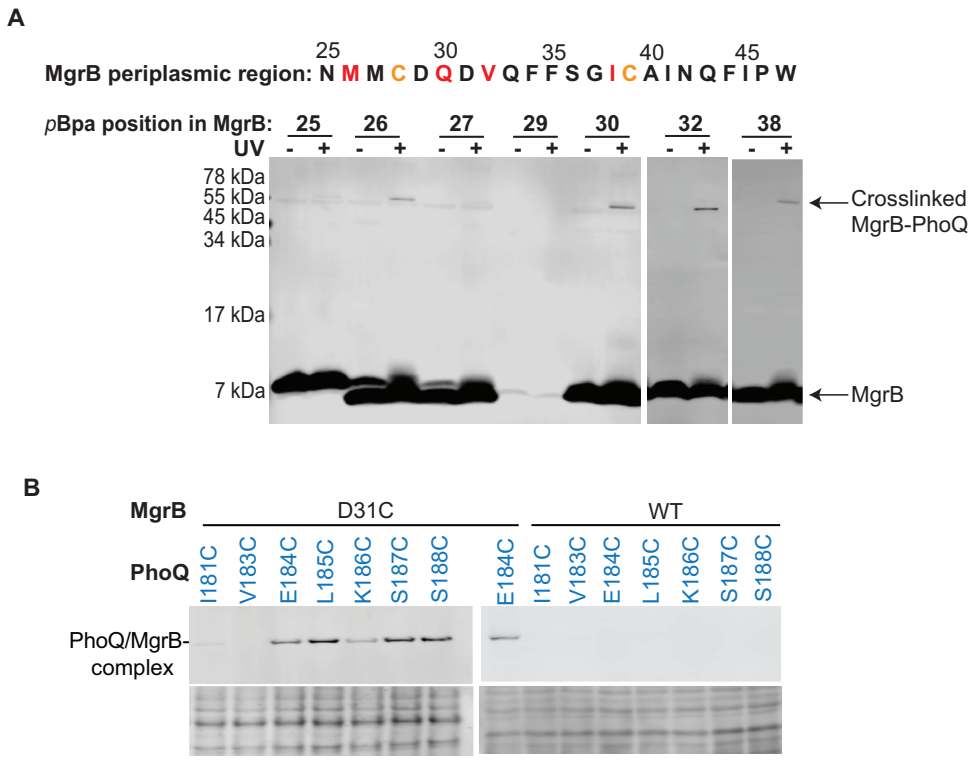

Fig. 2. Site-specific photo crosslinking in the periplasmic domain. (**A**) Western blot analysis of the site-specific photo crosslinking between PhoQ and MgrB. The *E. coli ΔphoQΔmgrB* strain harboring pETduet-1 *phoQ-his*$_6$ *flag-mgrB* and pEVOL-pBpF vectors were grown in LB containing the unnatural amino acid, *p*-benzoyl-l-phenylalanine (*p*BpA), which was incorporated into the FLAG tagged MgrB at the indicated positions via the amber stop codon and the cognate tRNA/aminoacyl-tRNA synthetase pair when inducing the expression of *flag-mgrB* and *phoQ-his*$_6$ from the plasmid. Cells were treated with UV light. The crosslinked MgrB-PhoQ complex was detected with Western blot using antibodies directed to the FLAG epitopes. Samples without UV irradiation served as controls. The residues showed UV crosslinking are colored in red in the MgrB sequence. Two conserved periplasmic cysteines are in yellow. (**B**)Western blot analysis of disulfide crosslinking from MgrB residue 31 to the PhoQ linker region connecting the periplasmic domain to the TM2 helix. The experimental procedures are as in Fig. 1C and details can be found in Materials and Methods. Data are representative of at least three independent experiments.

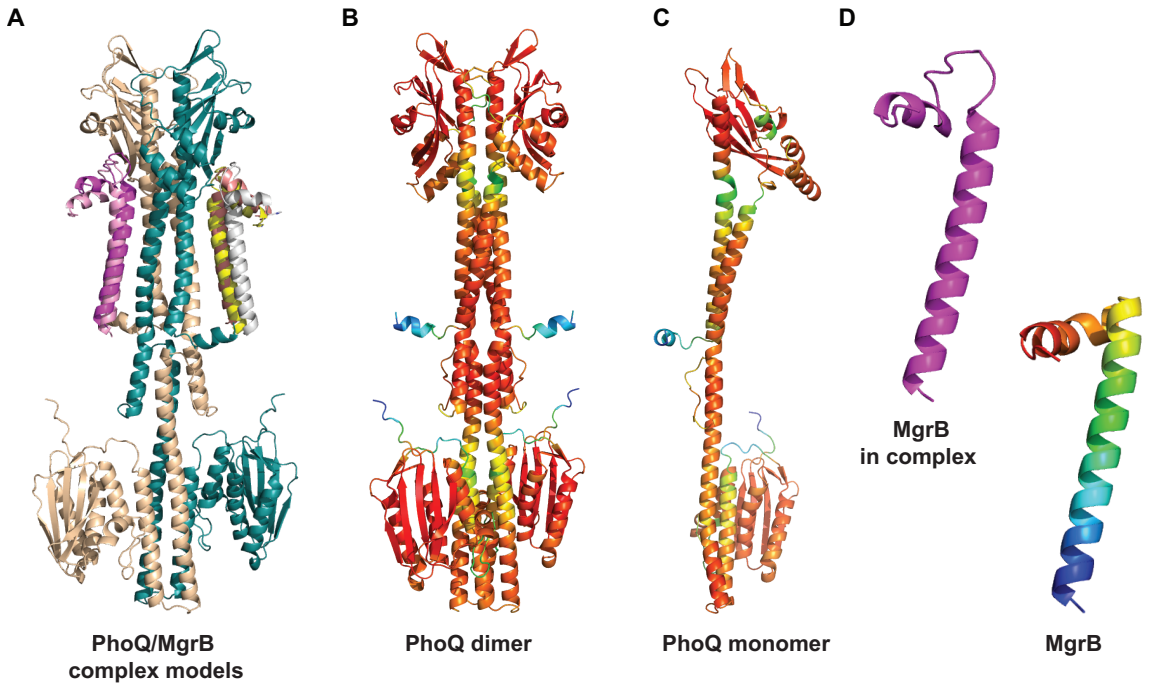

Fig. 3. Structural models predicted by Alphafold2. (**A**)The top five PhoQ/MgrB complex models are shown with a PhoQ dimer (colored in wheat and deep teal) and five MgrB molecules, which are shown in magenta, pink, yellow, pink and grey in model 1 to 5. (**B-C**) The predicted PhoQ dimer and monomer are colored in pLDDT score to show the flexible regions in the molecule. Compared to the structure prediction of MgrB (D, rainbow), the MgrB in complex (D, magenta) shows a more extend loop region. All structural figures were prepared using PyMOL unless otherwise stated.

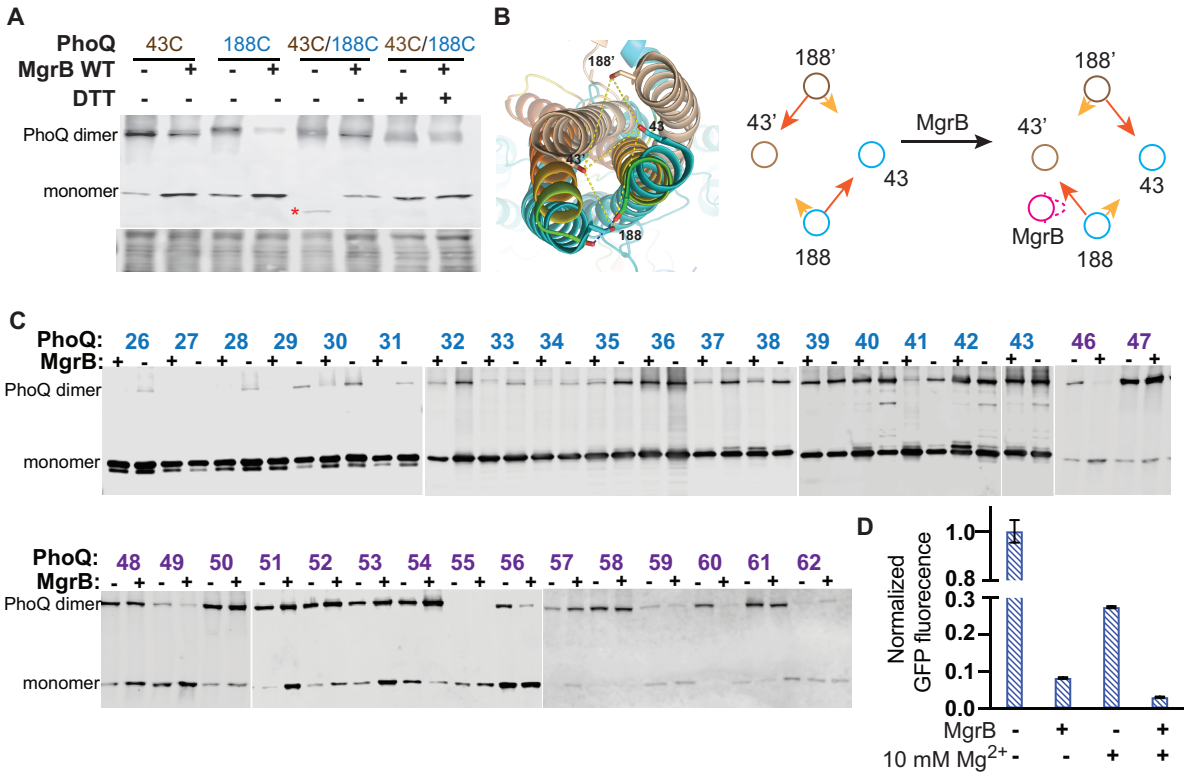

Fig. 4. The conformational change of the upon MgrB binding. (**A**) Western blot analysis of disulfide crosslinking within the PhoQ molecule in the presence or absence of MgrB. The His_6-tagged PhoQ cysteine variants were expressed with or without the wild type MgrB in *E. coli*. The disulfide crosslinking reaction was initiated with Cu-phenanthroline. The resulting crosslinked PhoQ species was then detected using Western blot with an anti-His antibody. The red asterisk indicates PhoQ molecules with an intramolecular disulfide crosslink. The total protein stain of the PVDF membranes below the Western blots serve as loading controls in A. Data are representative of three independent experiments. (**B,** left) The superimposition of the linker region in the PhoQ monomer (green) and dimer structures (wheat and blue). Residue 43 and 188 are shown with side chains in ball and stick. (**B,** right) A diagram of MgrB changing the disulfide crosslinking preferences between the cysteine residues at position 43 and 188. Brown and cyan circles represent the TM helices of the two monomers in the PhoQ dimer molecule. The magenta circle and curved dash line represent the TM helix and the loop region of MgrB, respectively. Orange arrows represent the crosslink tendency of the cysteine at position 188 to the cysteine at 43 in the same or the other PhoQ monomer. (**C**) MgrB induced PhoQ conformational change was detected via Western blot analyses of disulfide crosslinking along PhoQ dimer interface in the presence of MgrB. The His_6-tagged PhoQ cysteine variants were expressed with or without the wild type MgrB in *E. coli*. The experimental procedures are as described in A and details can be found in Materials and Methods. The position of cysteine is indicated as residue numbers in the PhoQ N-terminal helix. Blue and purple are residues in TM and periplasmic domain, respectively. Data are representative of three independent experiments. (**D**) The repression of PhoQ by high magnesium and MgrB. The function of PhoQ was monitored with the GFP reporter system using the *E. coli ΔphoQΔmgrB* strain as described in Fig. 1D. Data are representative of three independent experiments. Each data point is shown with the calculated average and standard deviation from three biological replicates.

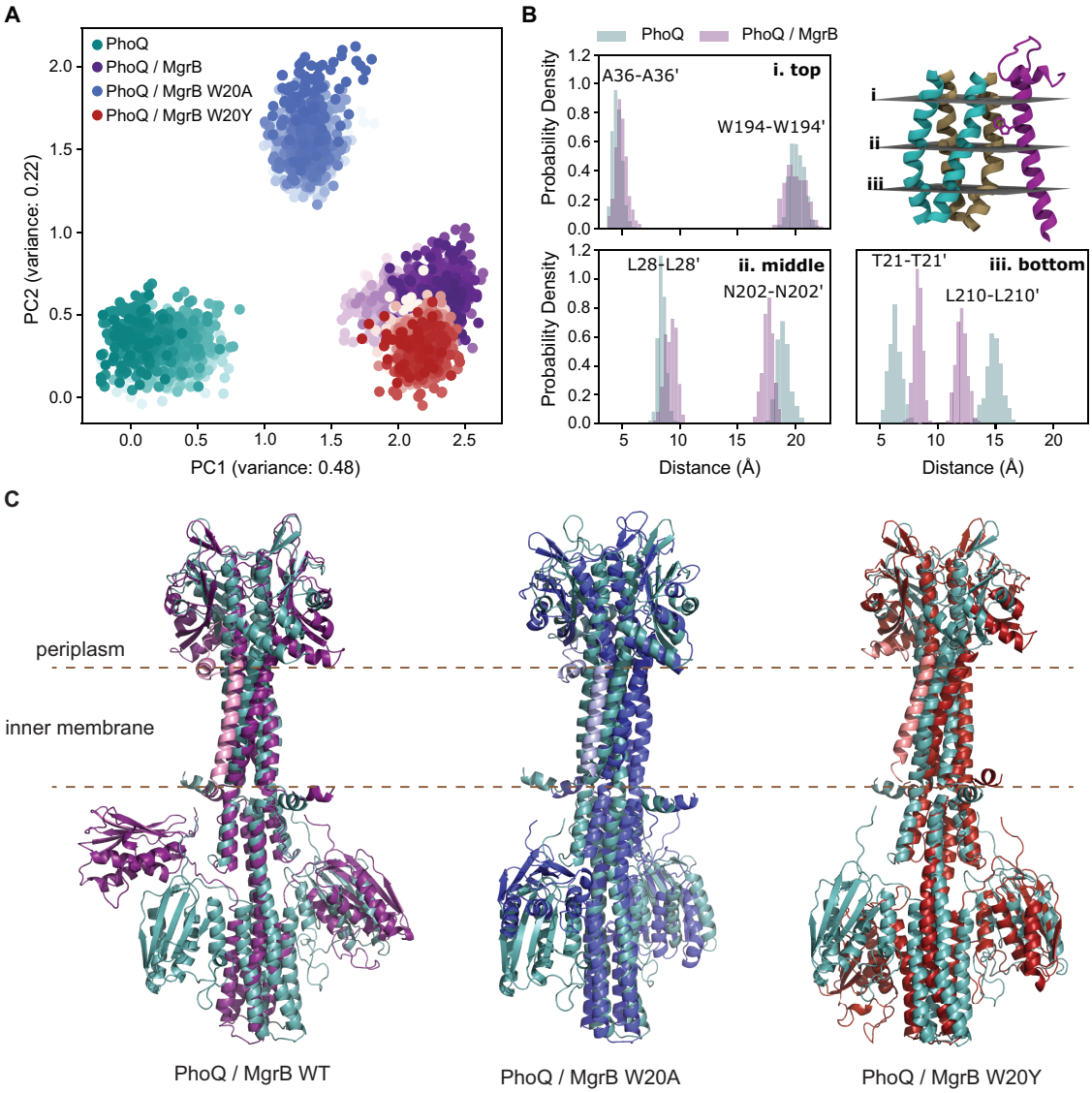

Fig. 5. MD simulations of PhoQ/MgrB complex models. (**A**) Projection of the molecular dynamics simulations into the eigenspace formed by the two first components of a Principal Component Analysis (PCA) of the transmembrane domain of PhoQ (residues 21 – 38 and 194 – 215). Each point corresponds to a conformation of the TM and is colored in shades of teal, purple, red and blue, for the simulations of PhoQ alone, and in complex with MgrB, MrgB W20Y and W20A, respectively. Lighter shades correspond to conformations sampled earlier in the simulation. (**B**) Distribution in distances between TM1 – TM1' (left) and TM2 – TM2' (right) at the top, middle, and bottom of PhoQ TM domain. (**C**) The overlay of the final conformations of PhoQ/MgrB complex models with PhoQ dimer. PhoQ structures are colored as in A. The MgrB wild-type, W20A, and W20Y variants are colored in pink, light blue, and light red, respectively.

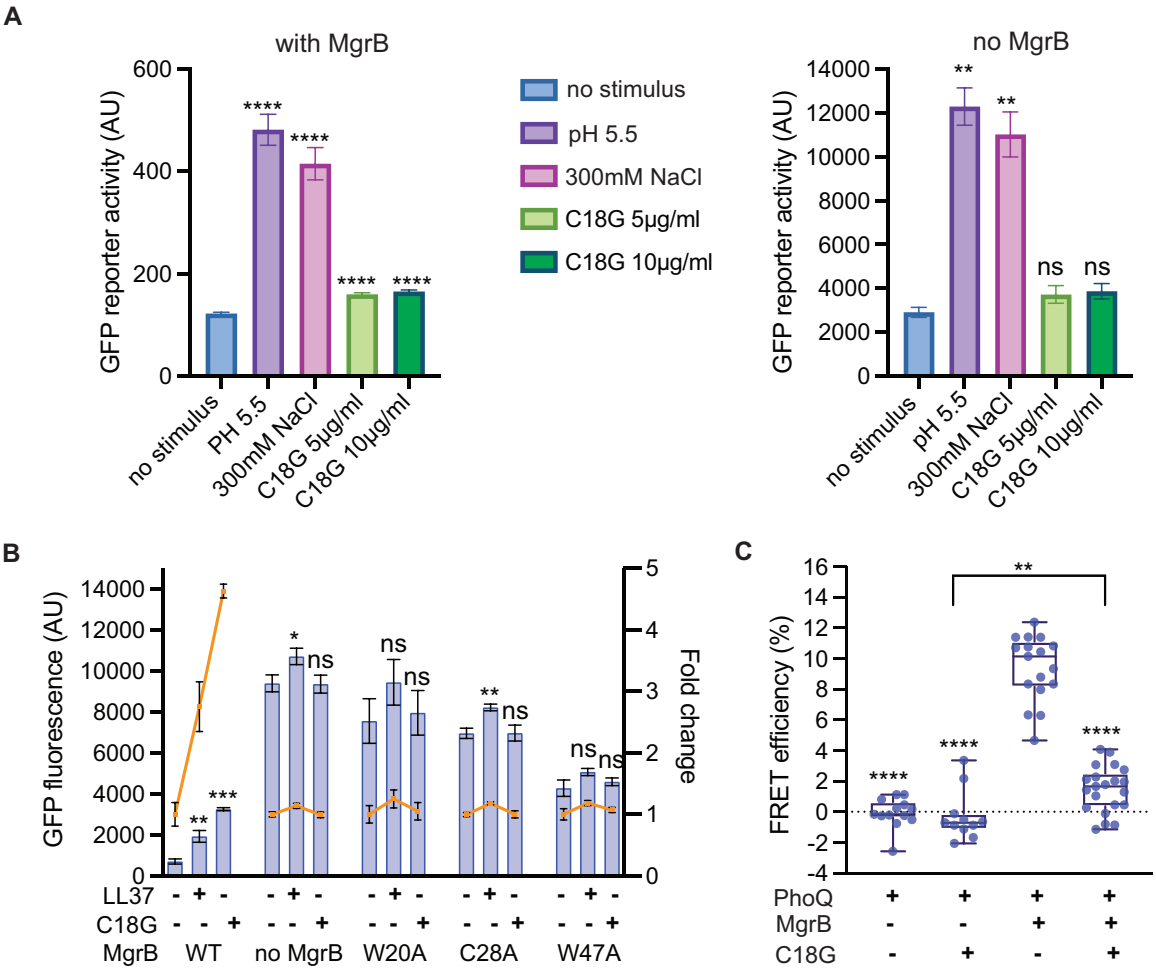

Fig. 6. MgrB mediates the antimicrobial peptide sensing by PhoQ. (**A**) The PhoQ activity assay with the GFP reporter system. *E. coli* MG1655 *ΔmgrB* strain harboring pBAD33 with (left panel) or without (right panel) *mgrB* gene, were induced with arabinose and grown in the presence of indicated stimuli in LB supplemented with 10 mM magnesium. (B) The activation of PhoQ in the presence of antimicrobial peptides and MgrB. *E. coli* MG1655 *ΔmgrB* strain expressing MgrB variants were grown in LB supplemented with 1 mM magnesium and antimicrobial peptides, LL37 or C18G as indicated. The PhoQ activity was followed by measuring the GFP fluorescence of the cell culture in A and B. Each data point is show with the calculated average and standard deviation from three independent biological replicates. (**C**) The FRET measurements of PhoQ-mNeonGreen and mCherry-MgrB *in vivo*. *E. coli* cells expressing PhoQ-mNeonGreen and mCherry-MgrB from plasmids were grown to mid log phase, then treated with or without the antimicrobial peptide, C18G. The energy transfer from mNeonGreen to mCherry was then measured for each condition. The strains expressing no FRET receptor (mCherry-MgrB) served as controls. Each data point is show with the calculated average and standard deviation from four independent experiments.

Table 1. The Cα - Cα distance of crosslinked residue pairs in the PhoQ/MgrB structural model.

Cα - Cα distance (Å)	W20-Y32	W20-L204	Q22-Y197	F24-I38
model 1	12.10	12.80	8.30	9.10
model 2	12.90	11.90	9.60	10.80
model 3	12.90	10.10	10.00	11.30
model 4	13.60	11.90	10.20	11.40
model 5	14.20	16.40	16.20	11.60